united nations educational, scientific and cultural organization

international atomic energy agency

the
abdus salam
international centre for theoretical physics

H4. SMR/1247
Lecture Note: 02

WORKSHOP ON PHYSICS OF MESOSPHERE-STRATOSPHERE-TROPOSPHERE INTERACTIONS WITH SPECIAL EMPHASIS ON MST RADAR TECHNIQUES

(13 - 24 November 2000)

AERONOMY AND DYNAMICS OF THE MESOSPHERE AND THE LOWER THERMOSPHERE STUDIED BY THOMSON SCATTER RADAR

Prof. Jurgen ROTTGER

Max-Planck-Institut fur Aeronomie
Katlenburg-Lindau
GERMANY

strada costiera, 11 - 34014 trieste italy - tel. +39 40 2240111 fax +39 40 224163 - sci info@ictp.trieste.it - www.ictp.trieste.it

AERONOMY AND DYNAMICS
OF THE MESOSPHERE
AND THE LOWER THERMOSPHERE
STUDIED BY
THOMSON SCATTER RADAR

Thomson scatter radars, usually called

Incoherent Scatter Radars

can be applied as useful ground-based tools
for studies of the ionosphere, the thermosphere
and the mesosphere

A Tutorial by
Jürgen Röttger
EISCAT Scientific Association
Kiruna, Sweden

Ninth International Symposium on Equatorial Aeronomy (ISEA)
Bali, Indonesia, 20-24 March 1995

E

Radar Observations of the Mesosphere

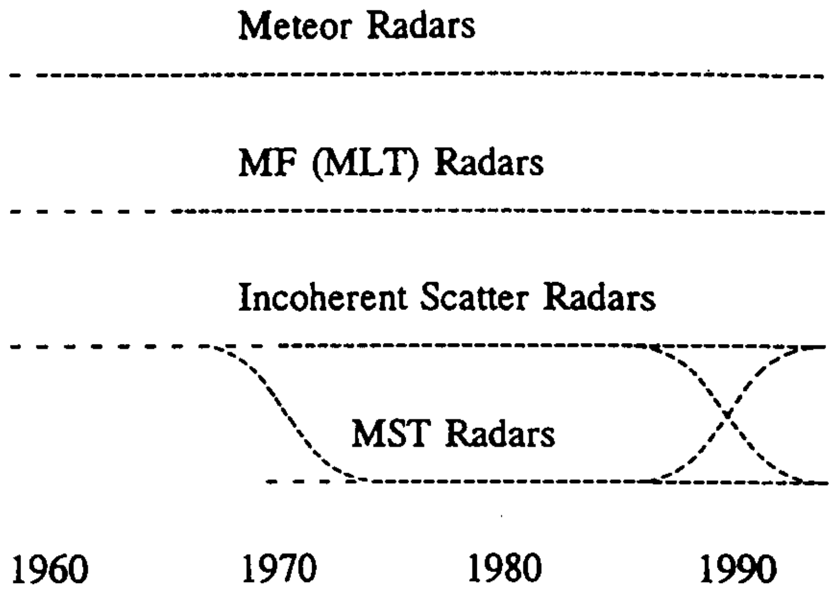

The MST Radars have evolved from the Incoherent Scatter Radars and more recently the interlacing of the scatter processes in the mesosphere governing these techniques has become evident.

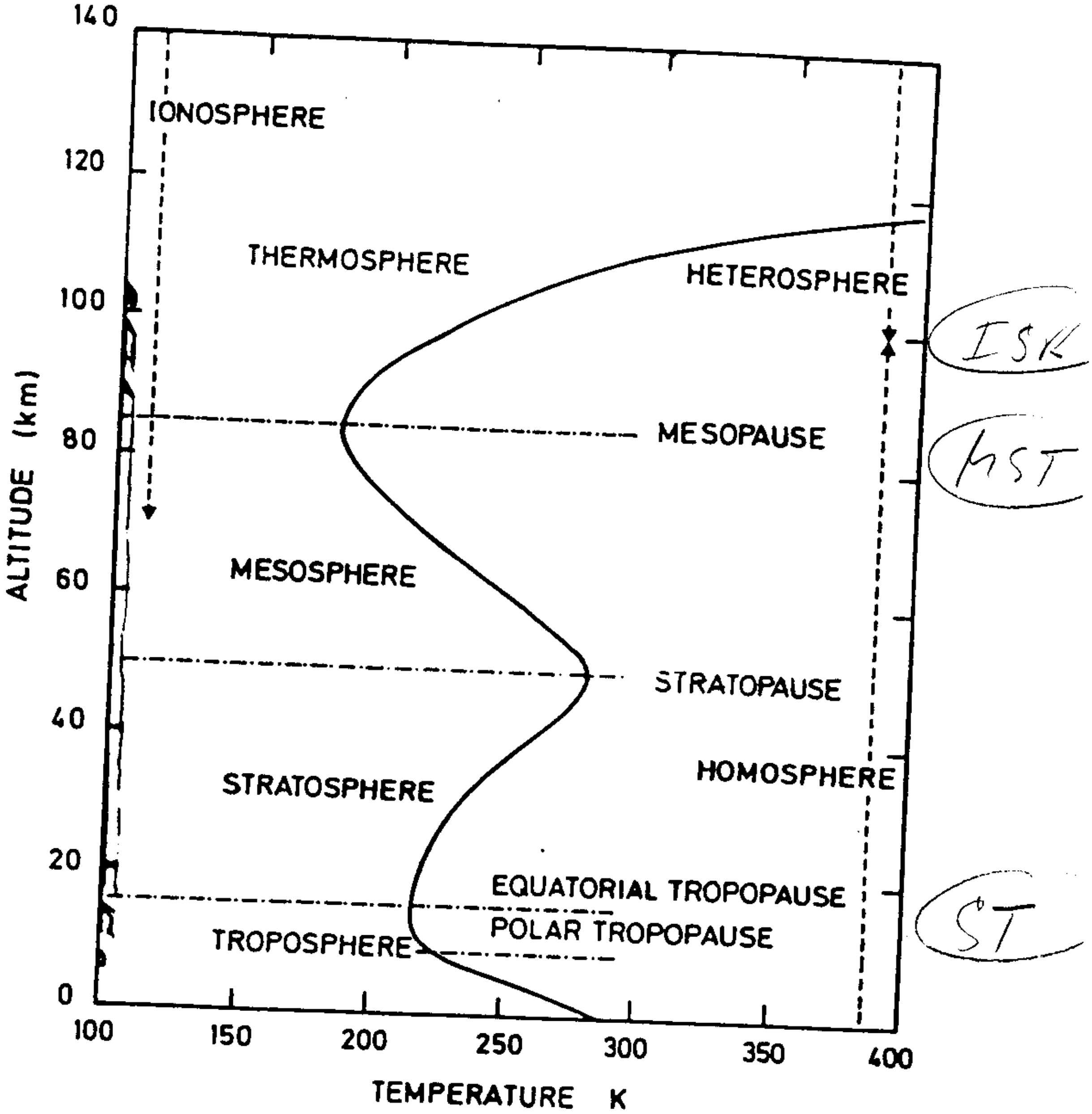
140
120
100
80
60
40
20
0
ALTITUDE (km)
100
150
200
250
300
350
400
TEMPERATURE K
IONOSPHERE
THERMOSPHERE
HETEROSPHERE
MESOPAUSE
MESOSPHERE
STRATOPAUSE
STRATOSPHERE
HOMOSPHERE
EQUATORIAL TROPOPAUSE
POLAR TROPOPAUSE
TROPOSPHERE
ISK
MST
ST

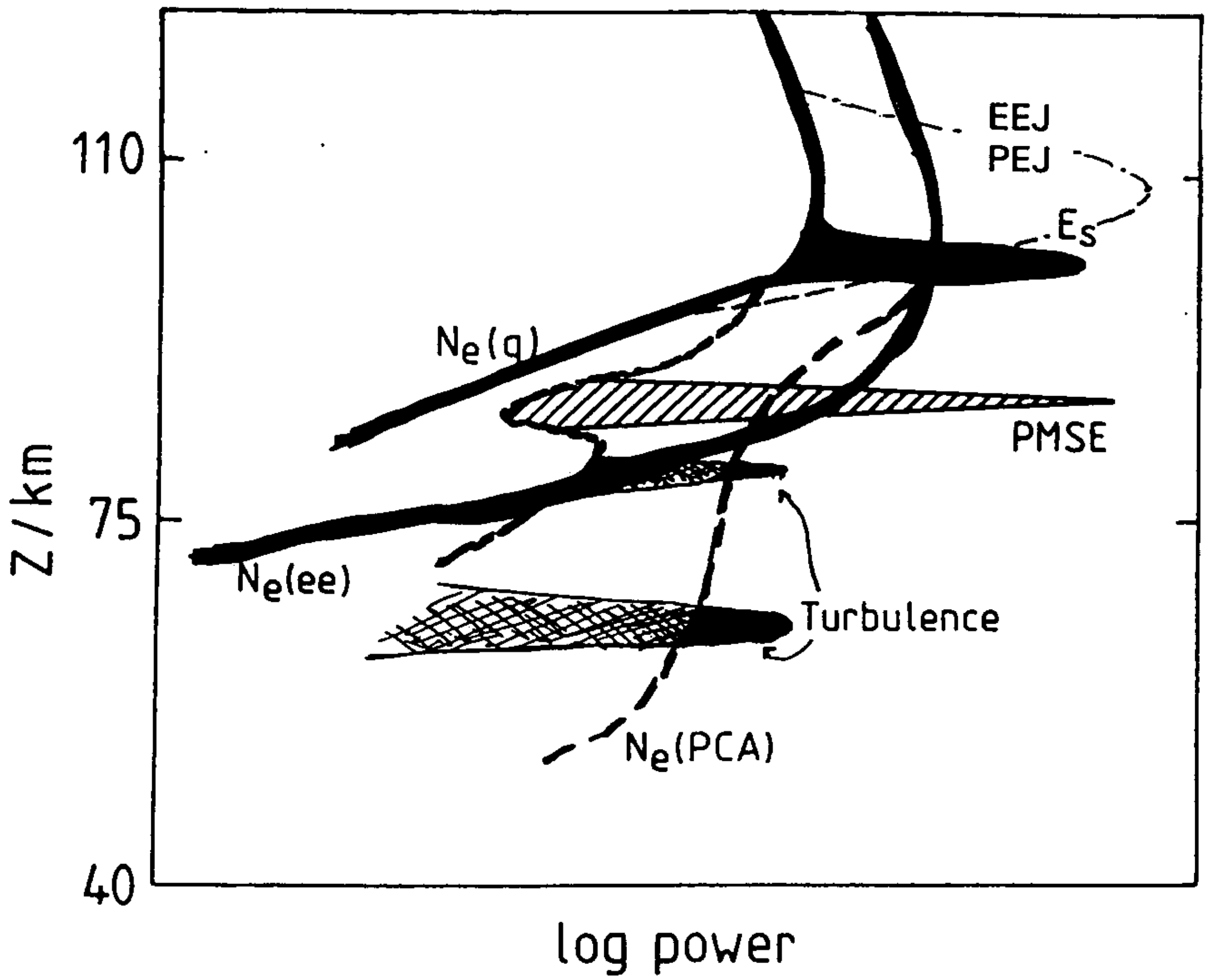

110
75
40
Z / km
log power
EEJ
PEJ
Es
Ne(q)
PMSE
Ne(ee)
Turbulence
Ne(PCA)

F03

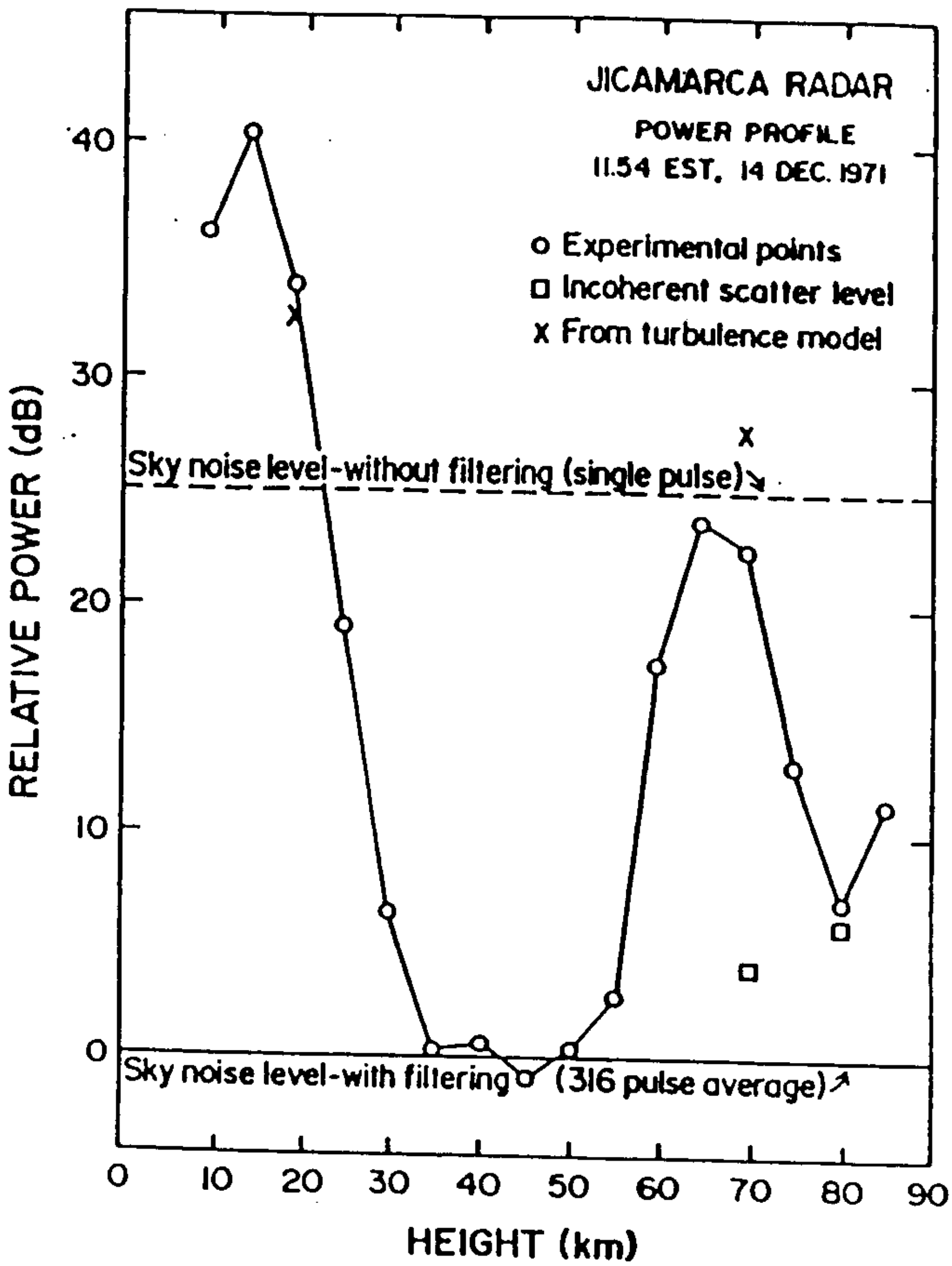

JICAMARCA RADAR
POWER PROFILE
11.54 EST, 14 DEC. 1971
o Experimental points
□ Incoherent scatter level
X From turbulence model
Sky noise level-without filtering (single pulse)
Sky noise level-with filtering
(316 pulse average)
RELATIVE POWER (dB)
HEIGHT (km)
0
10
20
30
40
50
60
70
80
90

F04

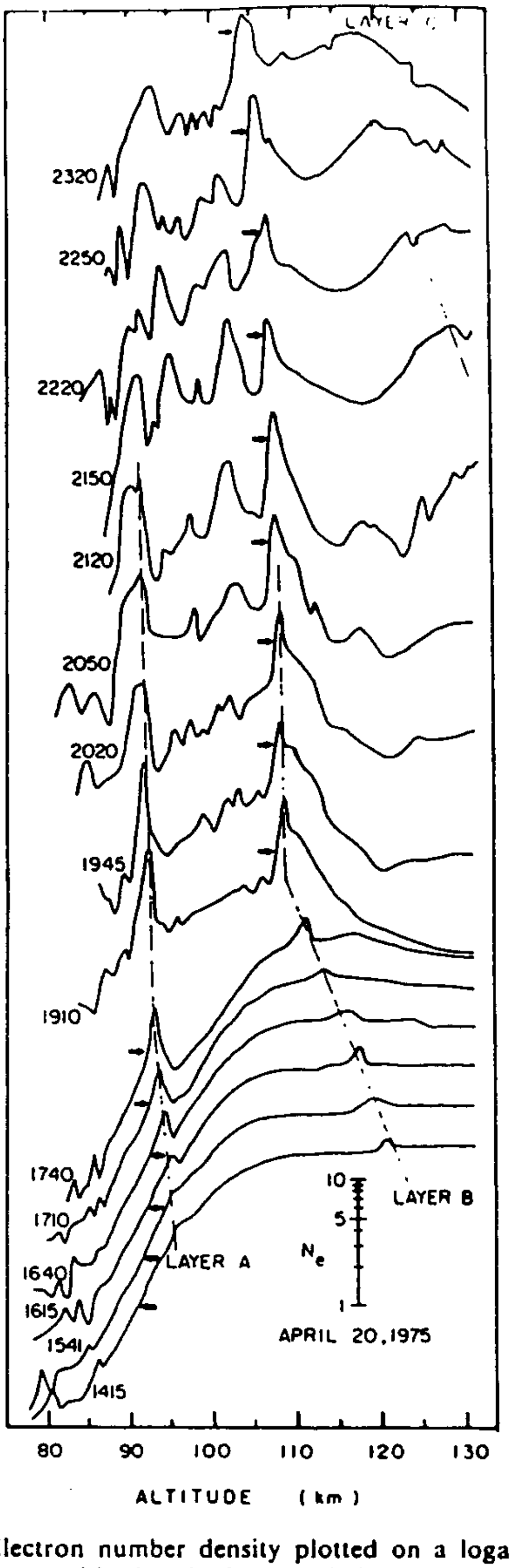

Fig. 1. Electron number density plotted on a logarithmic scale (ordinate) versus altitude (abscissa) and time (separate profiles arranged along the ordinate). The arrows indicate the 10^4 el/cm^3 level, and three separate long-lived layers (A, B, C) are indicated. Layer C is apparently a rapidly descending intermediate layer. Note the various rates of descent of the three layers.

MATHEWS AND BEKENY

EAC

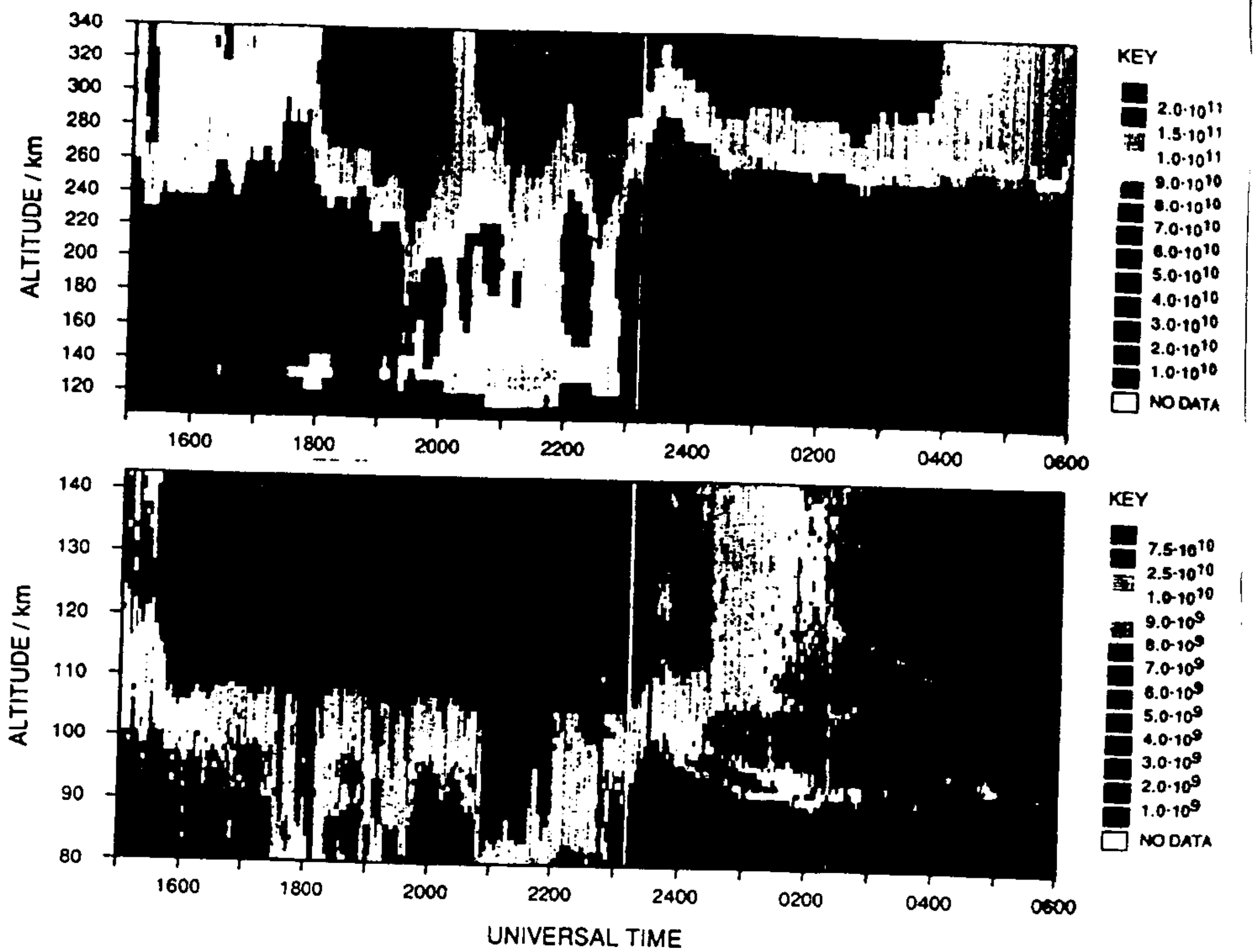

Electron density measured with Thomson scatter radar

EISCAT Tromsö, 9-10 December 1990
(T. Turunen et al., 1992)

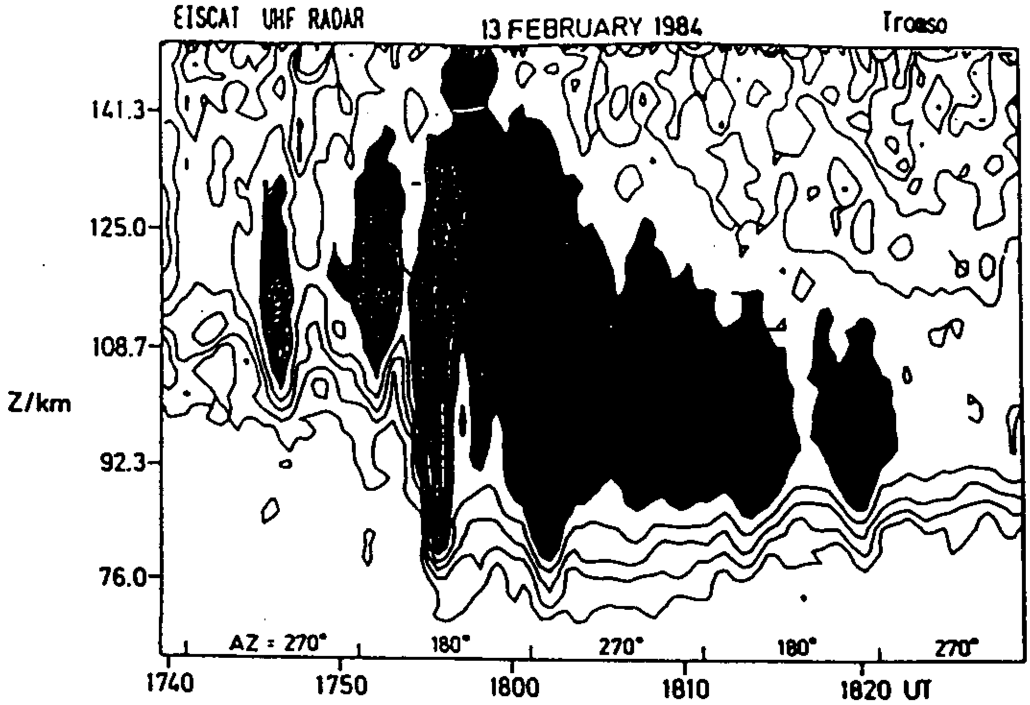

933 MHz
(a)

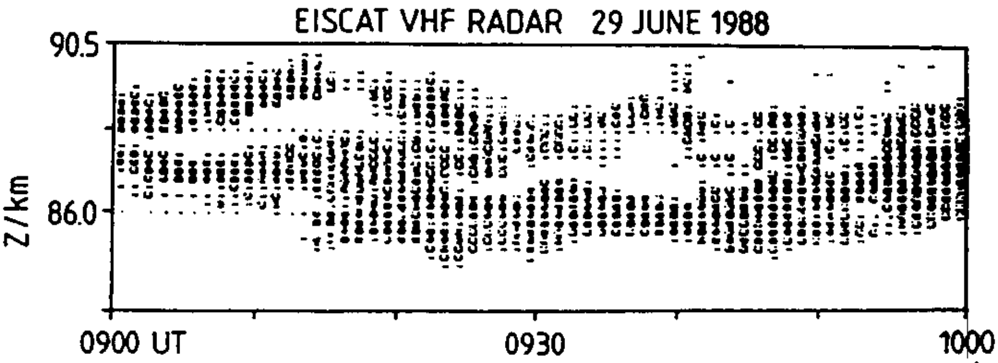

224 MHz
(b)

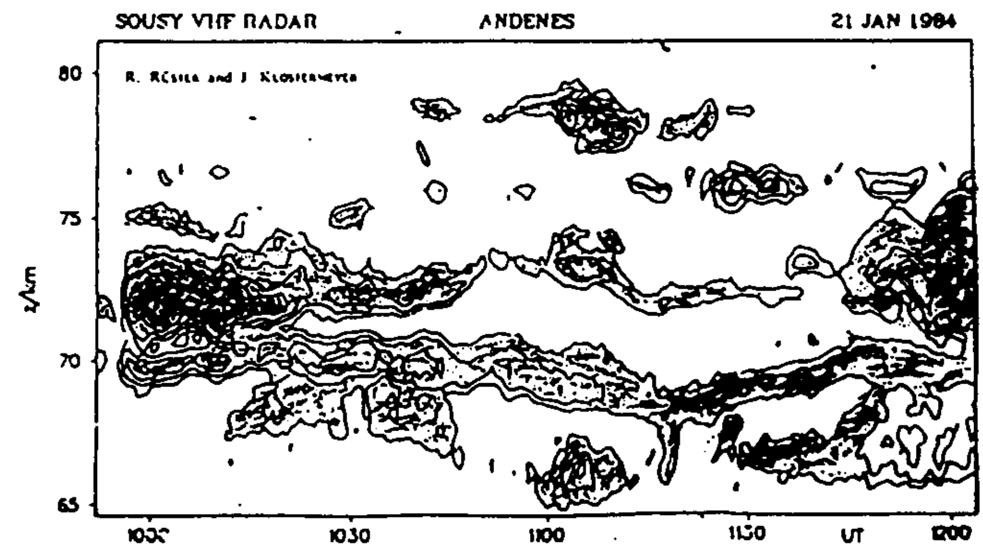

53 MHz
(c)

COHERENT SCATTER:

Variations in the refractive index of the lower atmosphere are caused by density, temperature and humidity variations, which are related to clear air turbulence and stable laminae.

The scattering process is called coherent because the scatterers have a quasi-deterministic structure.

Coherent scatter also occurs from ionisation irregularities which are caused by clear air tubulence in the mesosphere or by plasma instabilities in the ionospheric E- and F-regions.

INCOHERENT SCATTER:

If the plasma frequency
is smaller than
the radar frequency,
free electrons in the
ionosphere act as
Thomson scatterers,
and the scattered waves
from all electrons
in a unit volume
superimpose randomly.

E 09

Since the electrons are part
of the ionospheric plasma,
the ions also control the
scattering process.
In the middle atmosphere
the collisions between
neutral particles and
ionospheric plasma particles
are non-negligible and
the scattering process
is collision dominated.

The physical mechanism governing these two scattering processes is fundamentally the same, namely the backscattered power results from the constructive interference of electromagnetic waves scattered from variations of the refractive index at half the radar wavelength (so-called Bragg condition). Because of the weak scattering process, multiple scattering is neglegible.

Incoherent Scatter
is also called:

Thomson Scatter,
Thermal Scatter

It is characterized by an
"Overspread Spectrum" > 90 km
"Underspread Spectrum" < 90 km

Applied in:
Incoherent Scatter Radars
IS Radars

Coherent Scatter
is also called:

Irregularity Scatter,
Non-thermal Scatter,
Turbulence Scatter

It is characterized by an
"Underspread Spectrum"

Applied in:
E- and F-region irregularity backscatter radars, and in Mesosphere-Stratosphere-Troposphere Radars
MST Radars

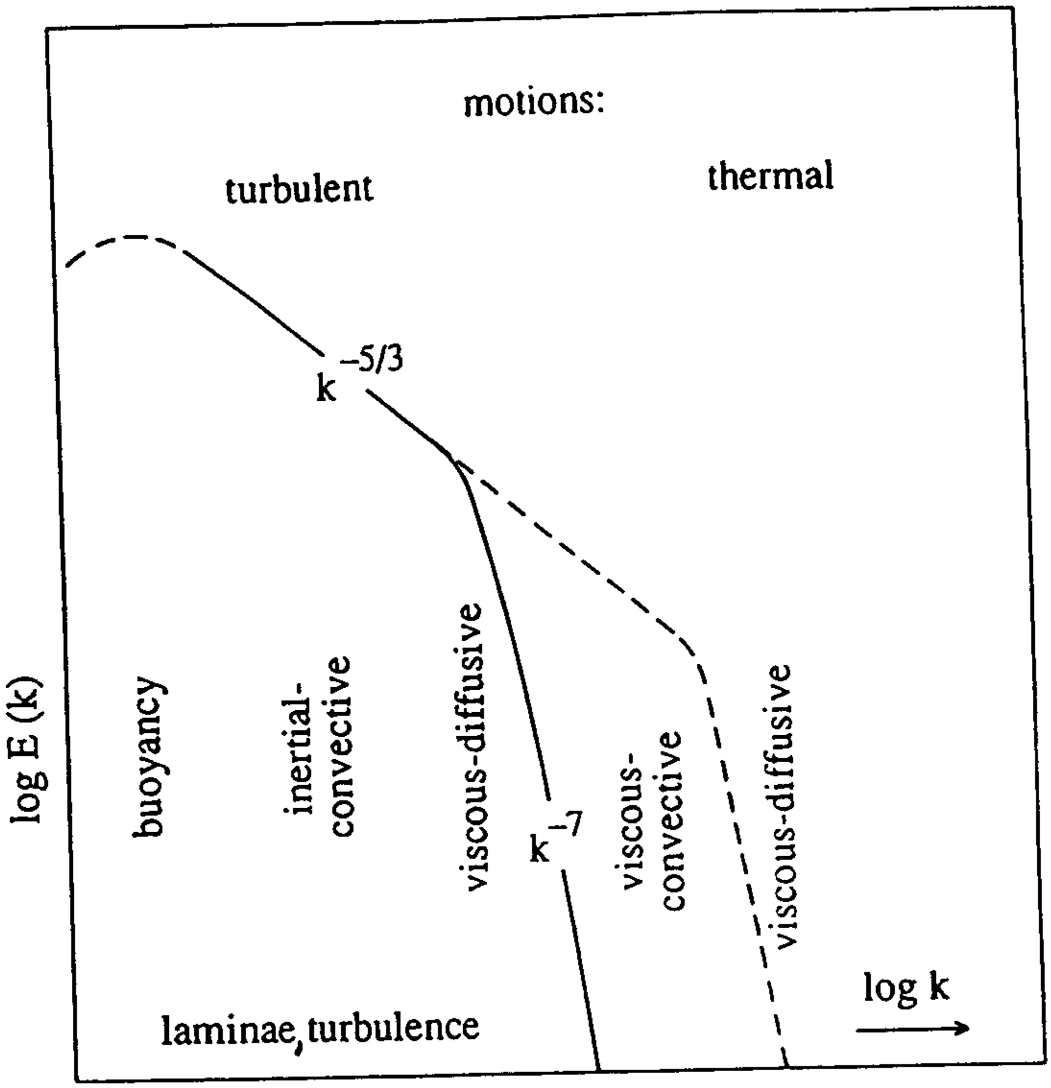

non-thermal
"coherent " scatter
MST scatter

thermal
"incoherent" scatter
Thomson scatter

E13

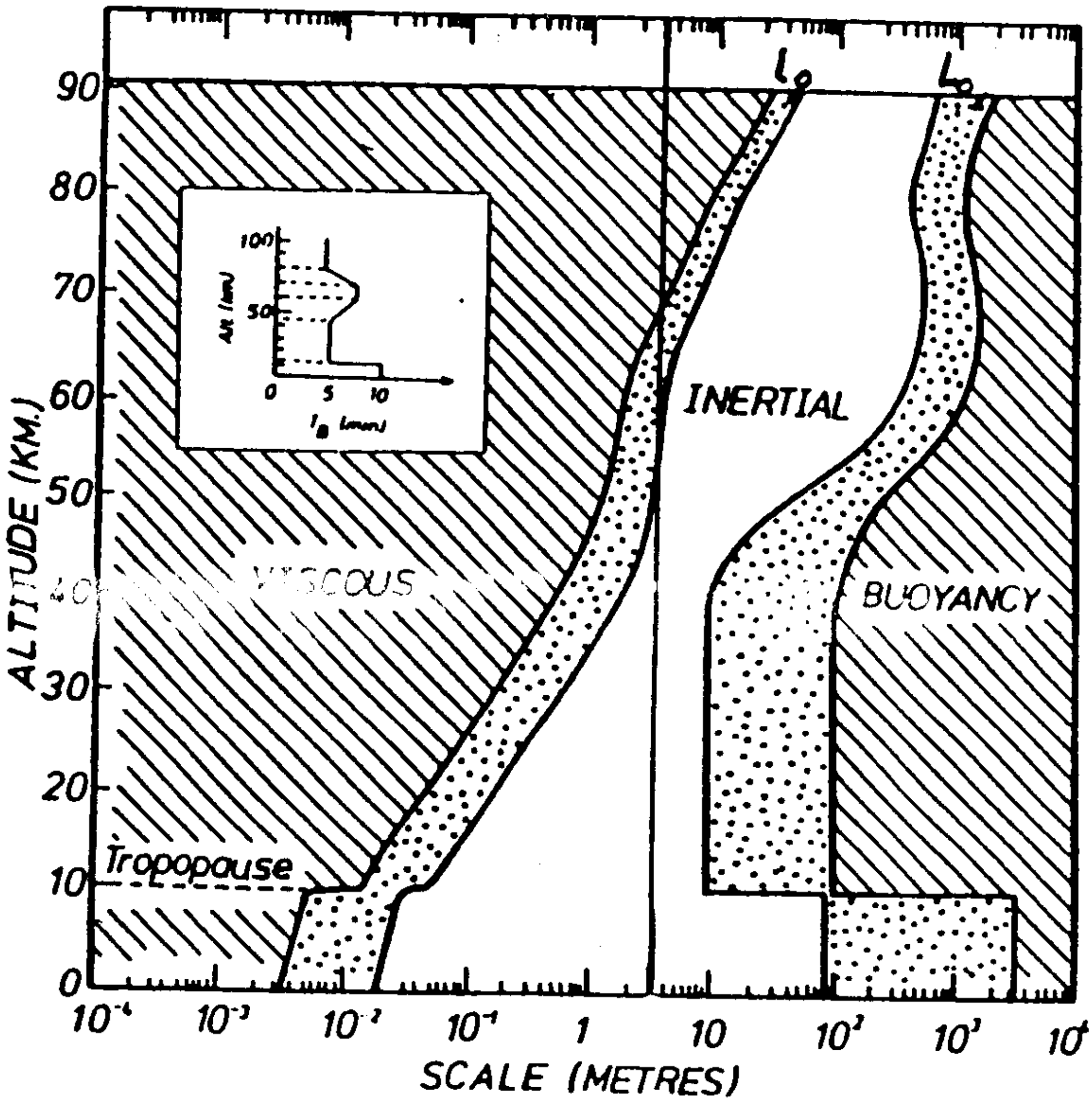

(from Hocking, 1983)

F10

Total backscattered power P_s

$$P_s = \frac{\alpha_e^2 A_e P_t \Delta r}{4\pi r^2} \cdot \sigma$$

The total scatter cross section is
in the mesosphere and lower thermosphere

$$\sigma = \sigma_t + \sigma_i$$

Depending on many, partially related, parameters

the scatter cross section for **MST**: σ_t

or the scatter cross section for **ISR**: σ_i

may dominate
and there is a transition region between both.

We will try to explain why this is the case and how one can discriminate between these components.

F 15

Scatter cross section of backscatter
from turbulence in the inertial subrange:

$$\sigma_t = 0.4\ C_n^2\ \lambda^{-1/3}$$

$$C_n^2 = 0.7\ \epsilon^{2/3}\ M^2\ \omega_B^{-2}\ F^{1/3}$$

$$M_m = \frac{r_e\ \lambda^2}{2\pi}\ (\ N_e\ (\frac{\omega_B^2}{g} - \frac{d\rho}{\rho\ dz}) - \frac{dN_e}{dz}\ )$$

E16

Scatter cross section of incoherent (Thomson) scatter:

$$\sigma_i = N_e \, \sigma_e$$

$$\sigma_e = 4 \, \pi \, r_e \left(\frac{\alpha^2}{1 + \alpha^2} + \frac{1}{(1 + \alpha^2) \cdot (1 + T_e / T_i + \alpha^2)} \right)$$

$$\alpha = \frac{\lambda}{2 \, \pi \, \lambda_D}$$

$$\lambda_D = 69 \cdot \left(\frac{T_e}{N_e}\right)^{1/2}$$

N_e = number density of free electrons

T_e = electron temperature,
assumed to be equal to ion temperature
and neutral temperature in the mesosphere

r_e = classical radius of electron (acting as
an individual 'Thomson scatterer' with
cross section of $0.998 \cdot 10^{-28}$ m^2)

λ_D = Debye length (ions forming a shielding
sphere around electron of radius λ_D)

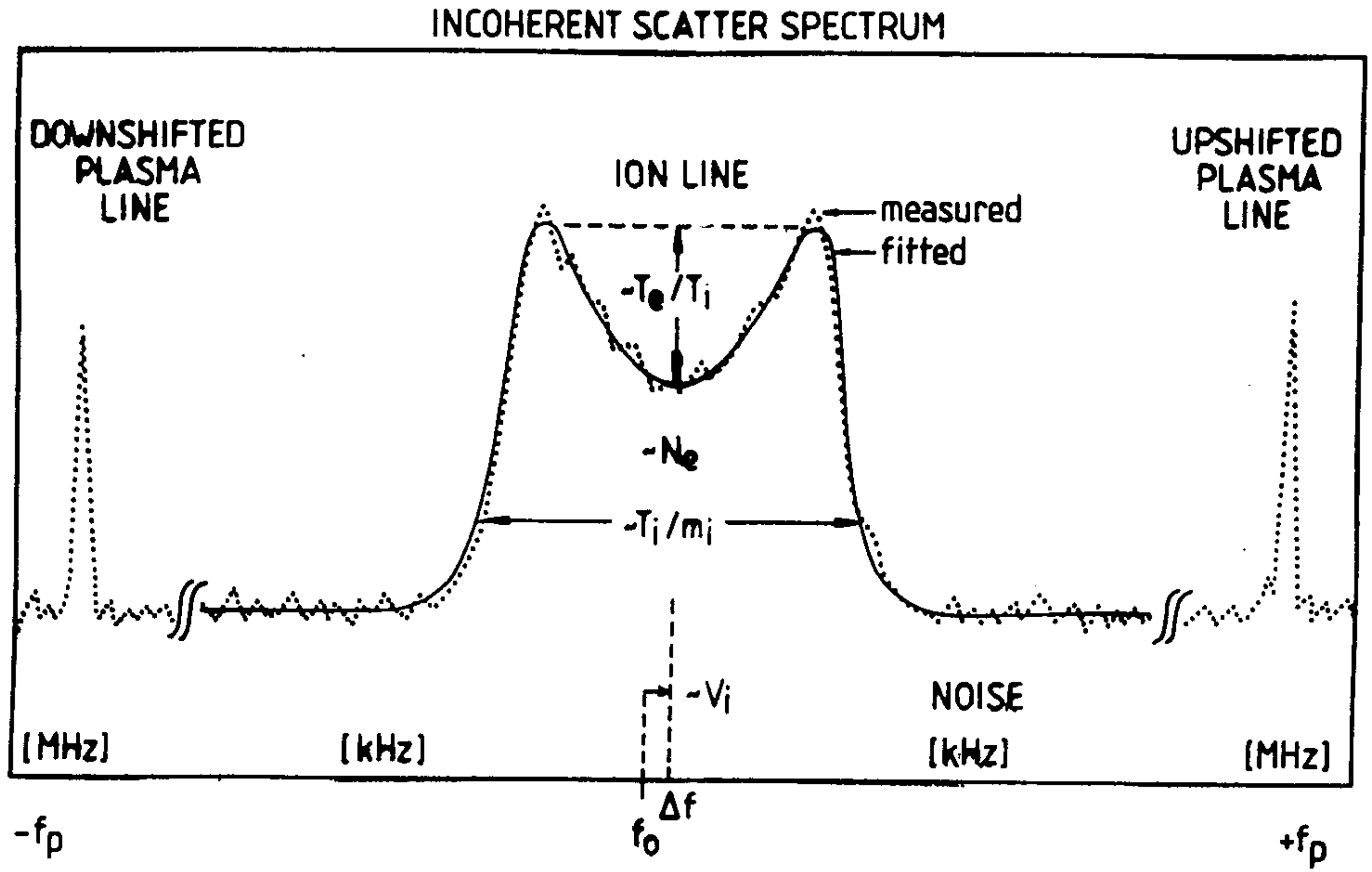
INCOHERENT SCATTER SPECTRUM
DOWNSHIFTED PLASMA LINE
ION LINE
measured
fitted
UPSHIFTED PLASMA LINE
~T_e/T_i
~N_e
~T_i/m_i
~V_i
NOISE
[MHz]
[kHz]
[kHz]
[MHz]
$-f_p$
f_o
Δf
$+f_p$

If the radar wavelength is much larger than the mean free path of the ions, the incoherent scatter is collision dominated, i.e. the ion motions are a replica of the motions of the neutral particles. The mean free path is given by the collision frequency ν_i of the ions and the neutrals.

The condition of collision dominated incoherent scatter is determined by the ratio of radar wavelength λ and the mean free path, which is also called the normalized collision frequency:

$$\psi_i = \frac{\lambda\ \nu_i\ m_i^{1/2}}{4\ \pi\ (2\ k_B\ T_i\ )^{1/2}}$$

The incoherent scatter from the mesosphere is usually collision dominated, since $\Psi_i >> 1$.

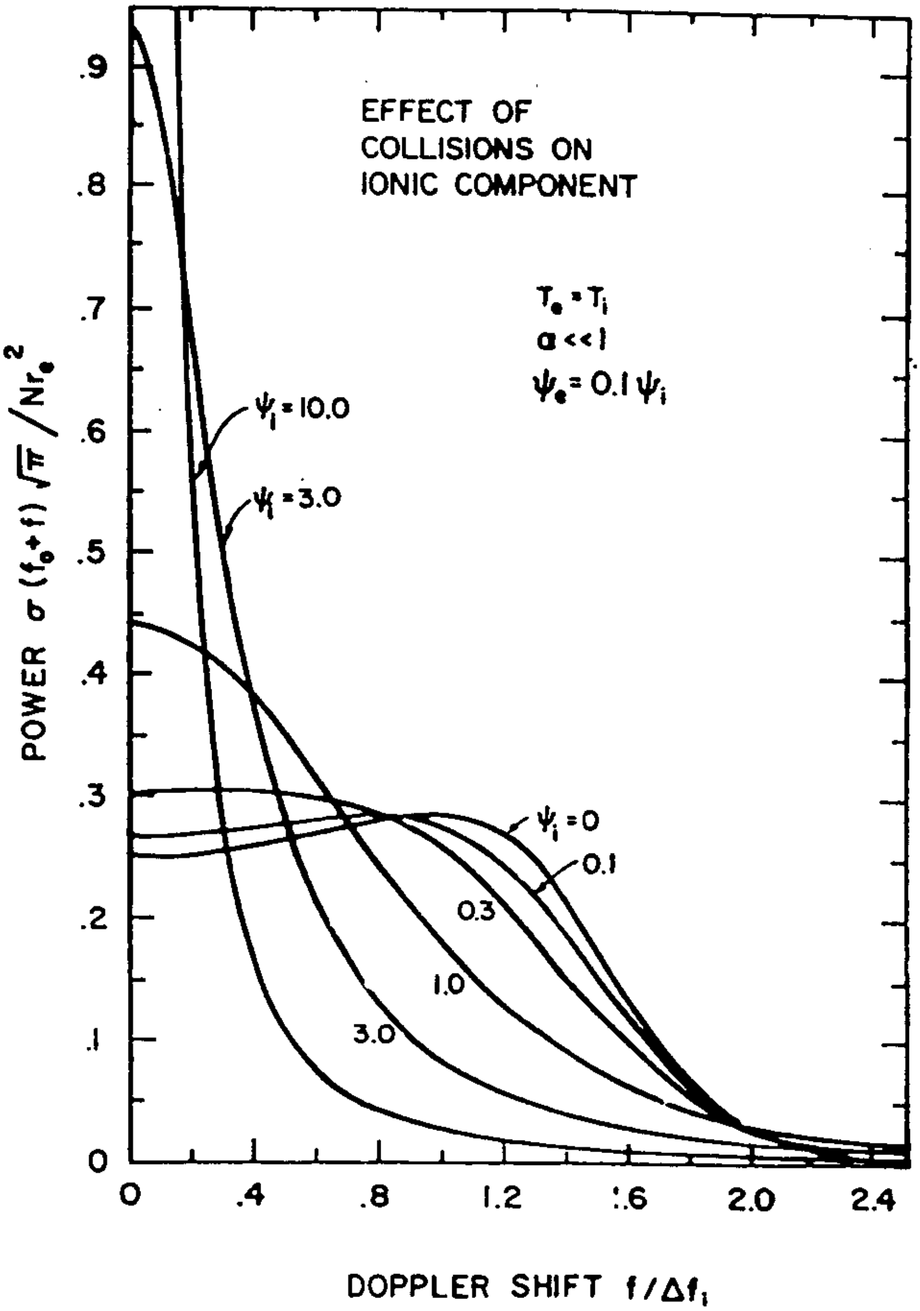

EFFECT OF
COLLISIONS ON
IONIC COMPONENT
$T_e = T_i$
$\alpha << 1$
$\psi_e = 0.1\,\psi_i$
$\psi_i = 10.0$
$\psi_i = 3.0$
$\psi_i = 0$
0.1
0.3
1.0
3.0
POWER $\sigma(f_0+f)\sqrt{\pi}/Nr_e^2$
DOPPLER SHIFT $f/\Delta f_i$

F2

The presence of negative ions also increases the scatter cross section (Fukuyama and Kofman, 1980):

$$\sigma = \frac{4 \pi N_e r_e^2 (\alpha^2 (1 + 2 \lambda^-) + 1)}{2 (1 + \lambda^-) \alpha^2 + 1}.$$

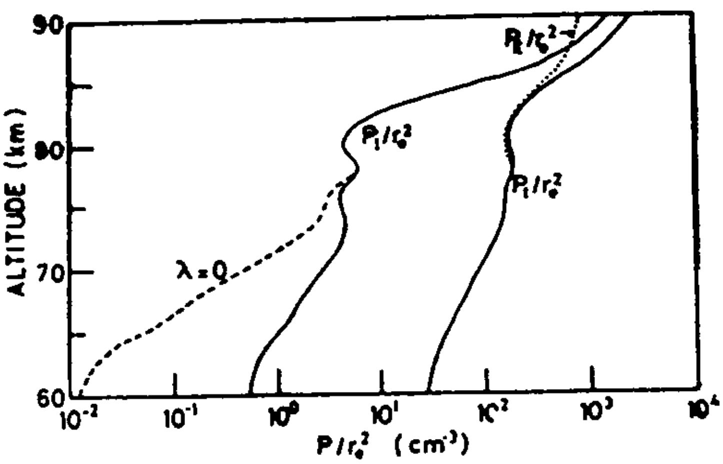

Fig. 7. Vertical profiles of the total cross sections calculated with and without negative ions.

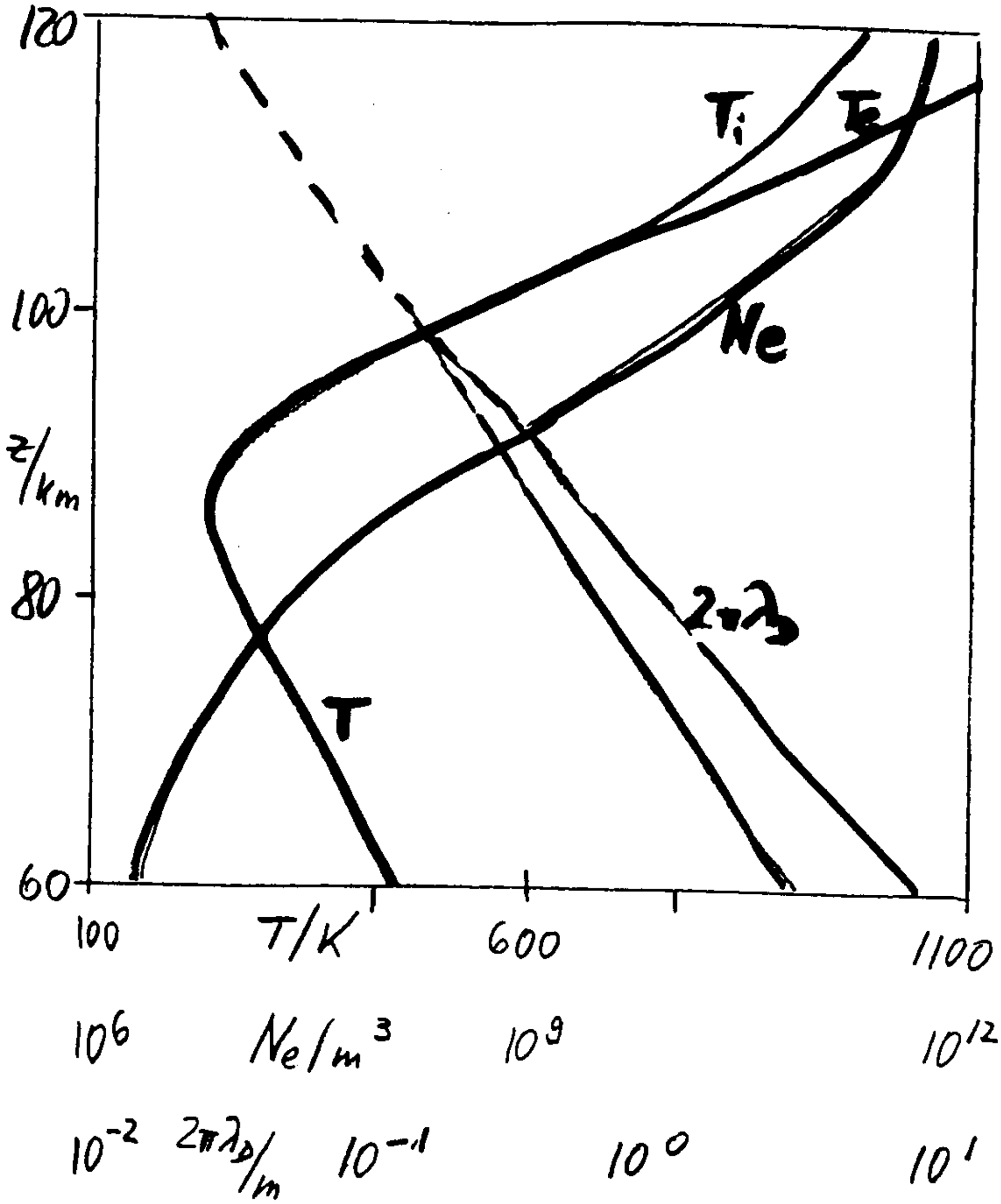

$$\lambda_D \propto \sqrt{T_e/N_e}$$

$$\lambda_{radar} \gg \lambda_D$$

The spectrum width f_s of an incoherent scatter signal from a collision dominated plasma (mesosphere) is given by:

$$f_s = \frac{32\ \pi^2\ k_B}{\lambda^2}\ \frac{T}{m_i\ \nu_i}\ \frac{2\ (\ 1 + \lambda^-\ ) + \alpha^2}{(\ 1 + \alpha^2\ )}$$

λ^- is the ratio of negative ions and electrons

k_B is the Boltzmann constant

m_i is the mass of ions

ν_i is the ion-neutral collision frequency

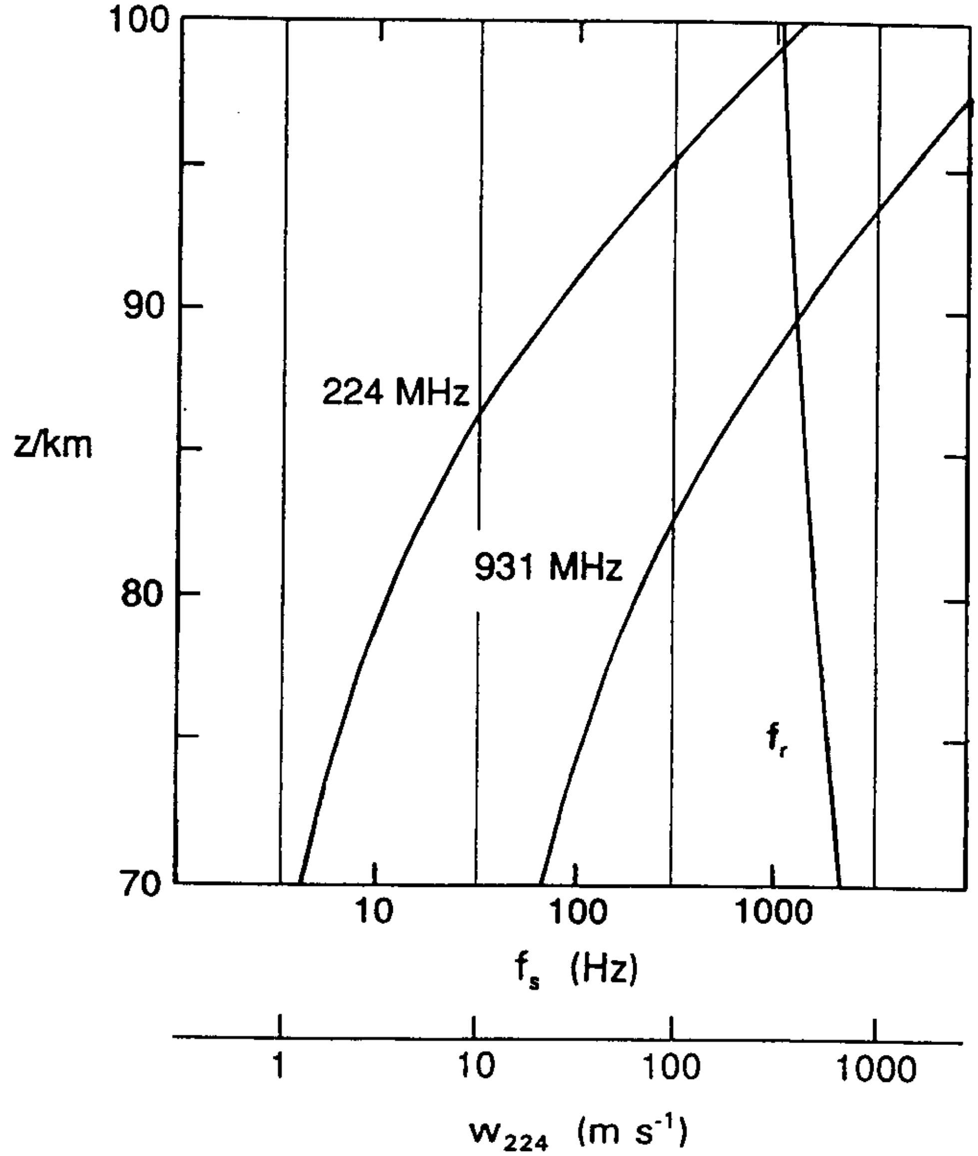

$f_w^2 = f_s^2 + f_t^2$

effect on width

below ≃ 80 km

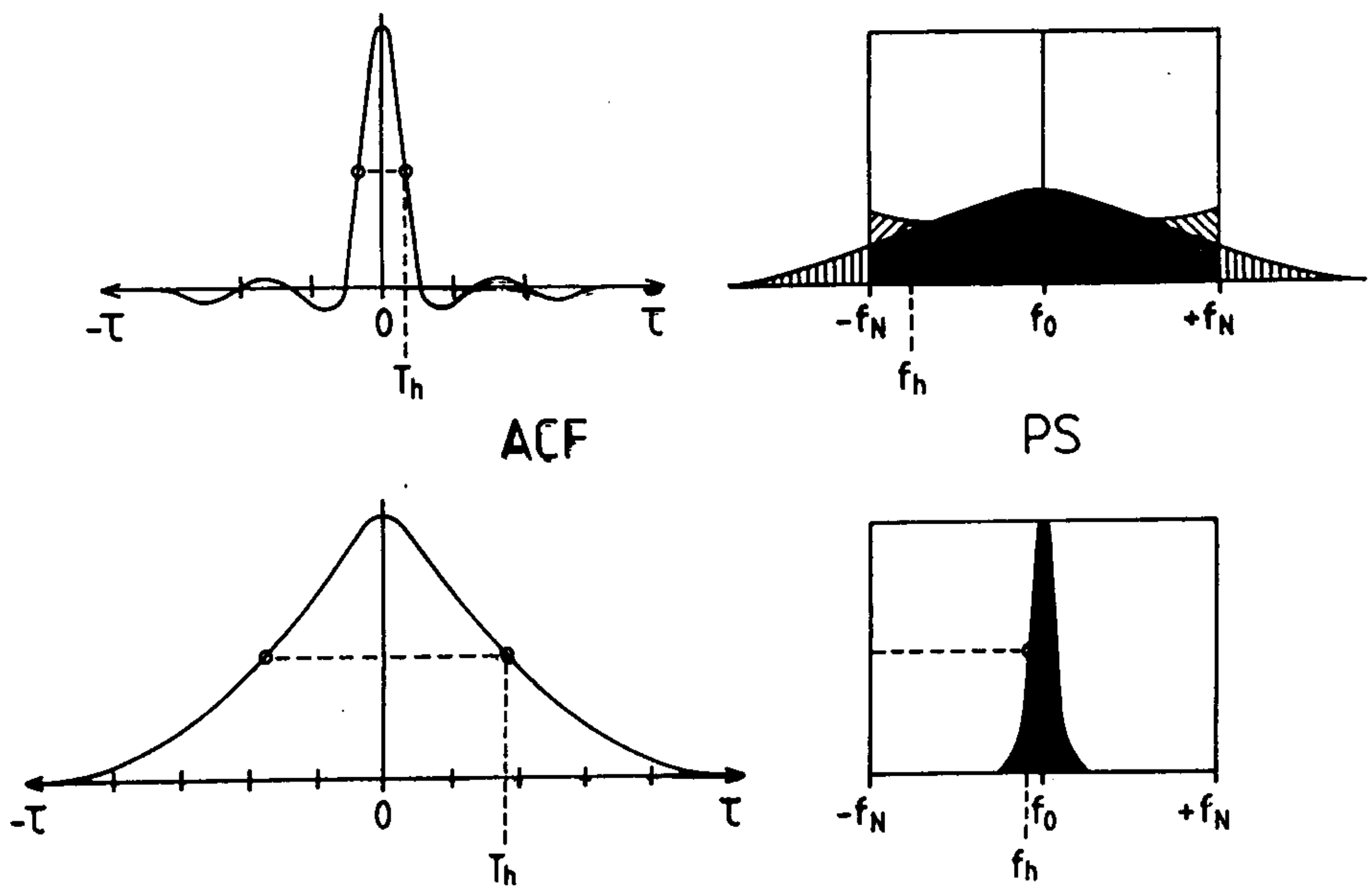

-τ
0
τ
T_h
$-f_N$
f_0
$+f_N$
f_h
ACF
PS

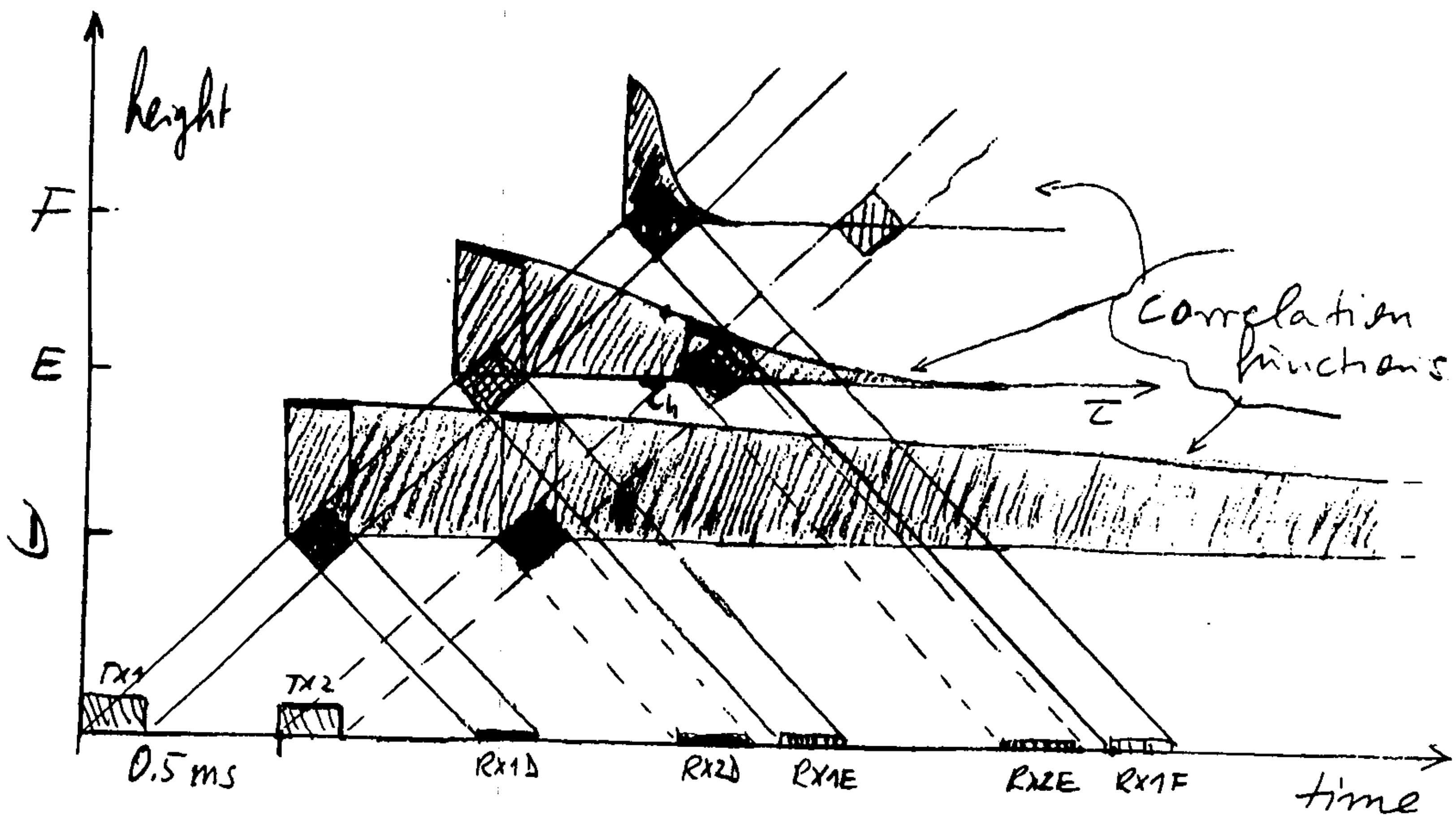
height
F
E
D
TX1
TX2
0.5 ms
RX1D
RX2D
RX1E
RX2E
RX1F
time
τ
correlation functions

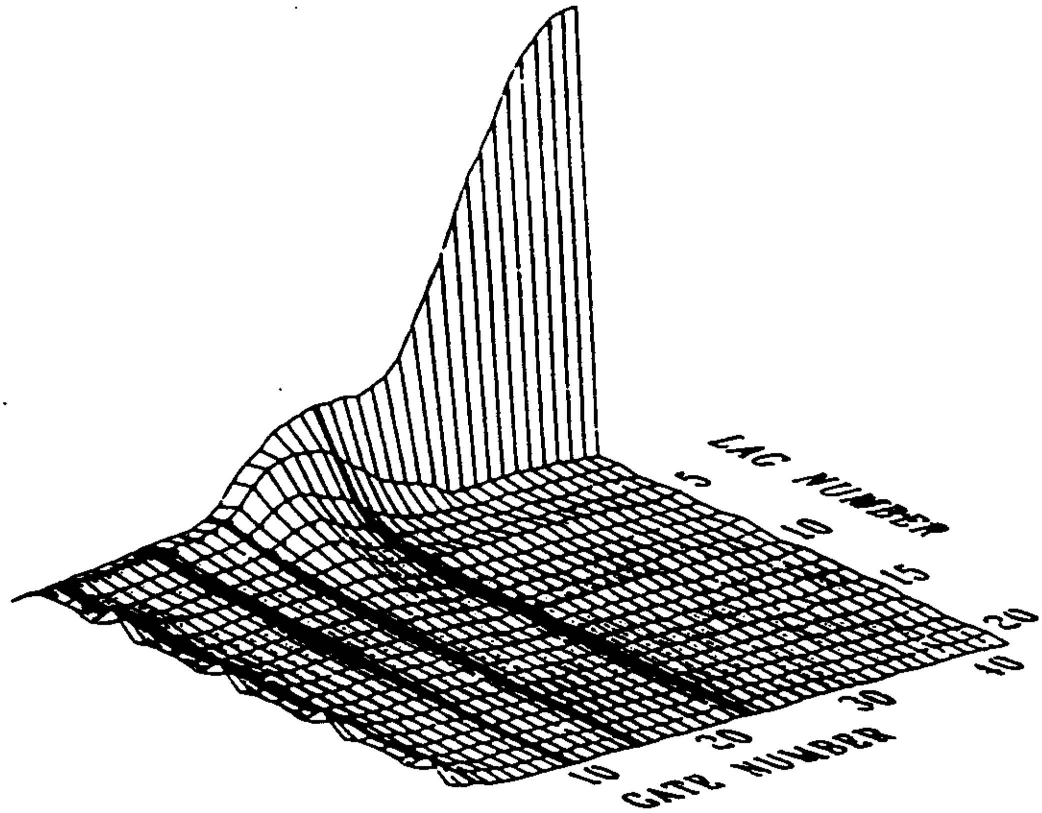

Fig. 7. A perspective plot of the autocorrelation functions measured on 27 April 1987 at 22:10–22:30 UT.

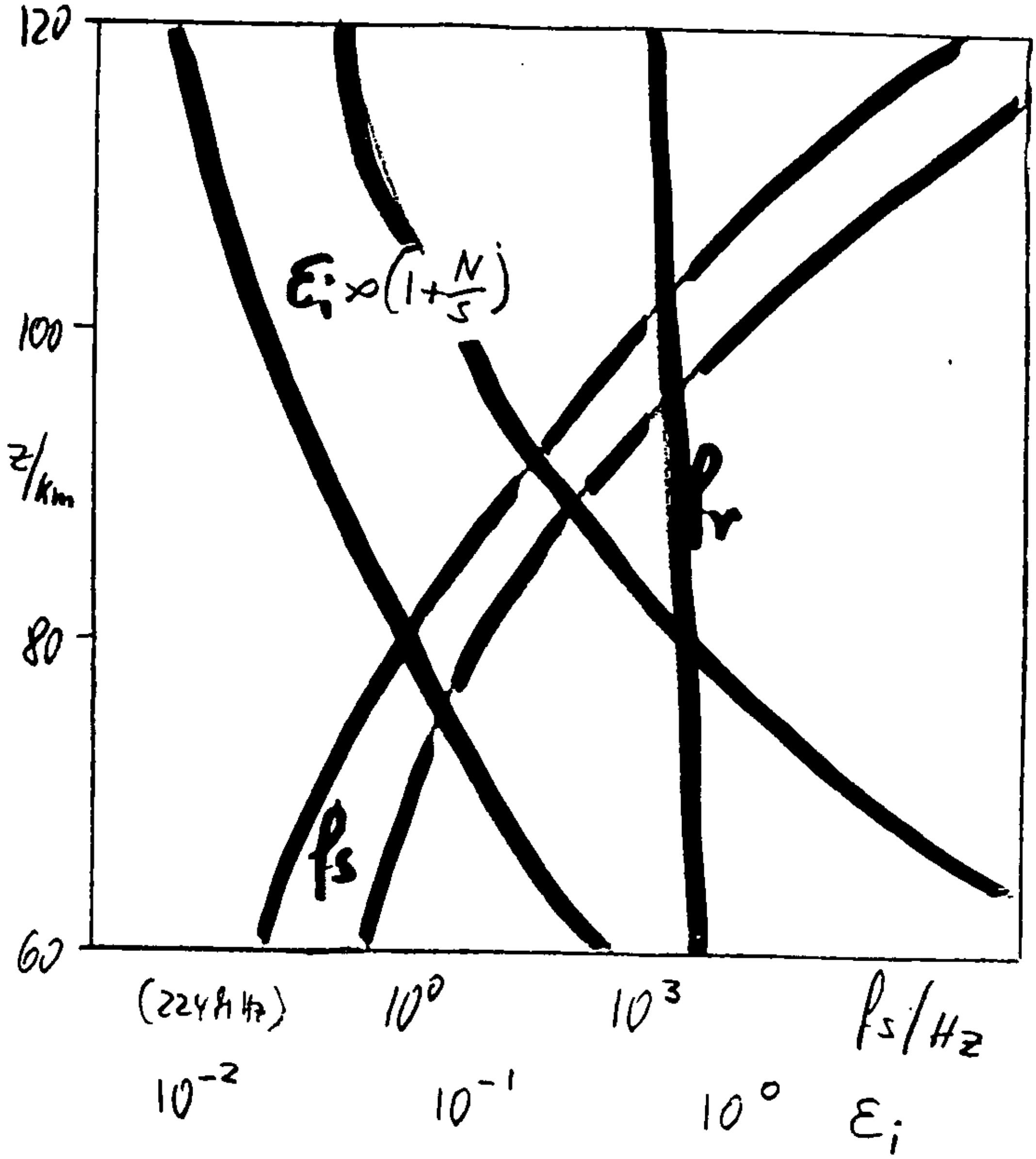

E28

Arecibo, 10 Aug 1979 10 AST - 10 45 AST

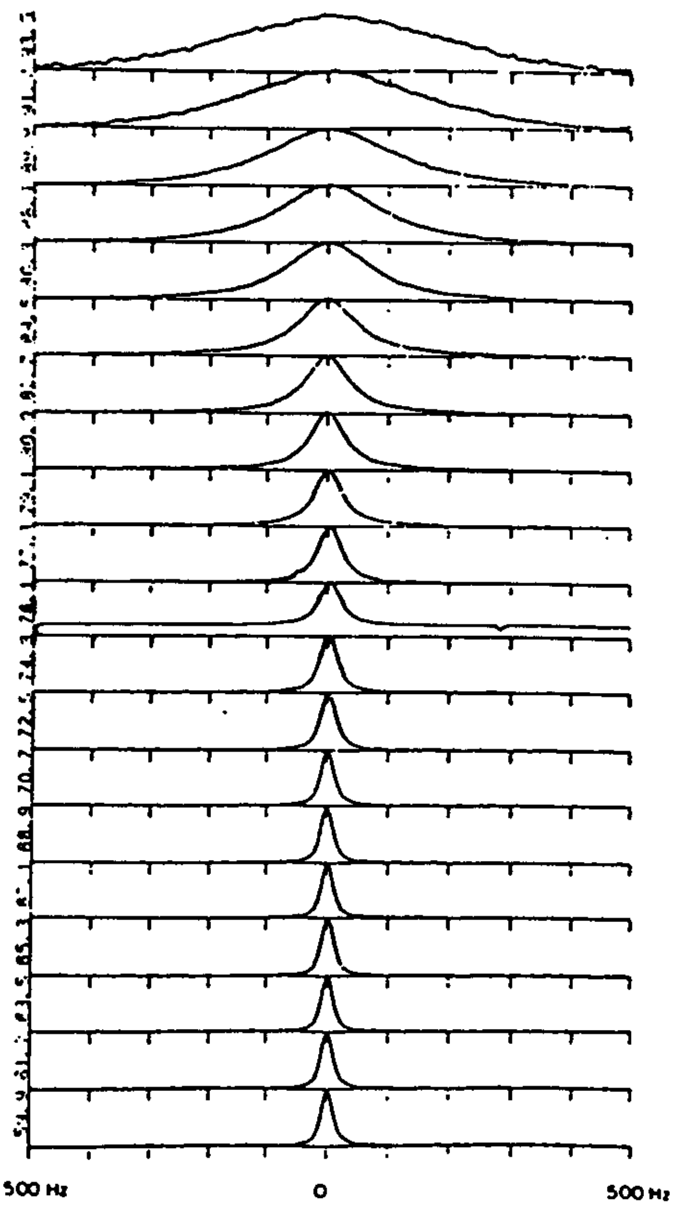

E 29

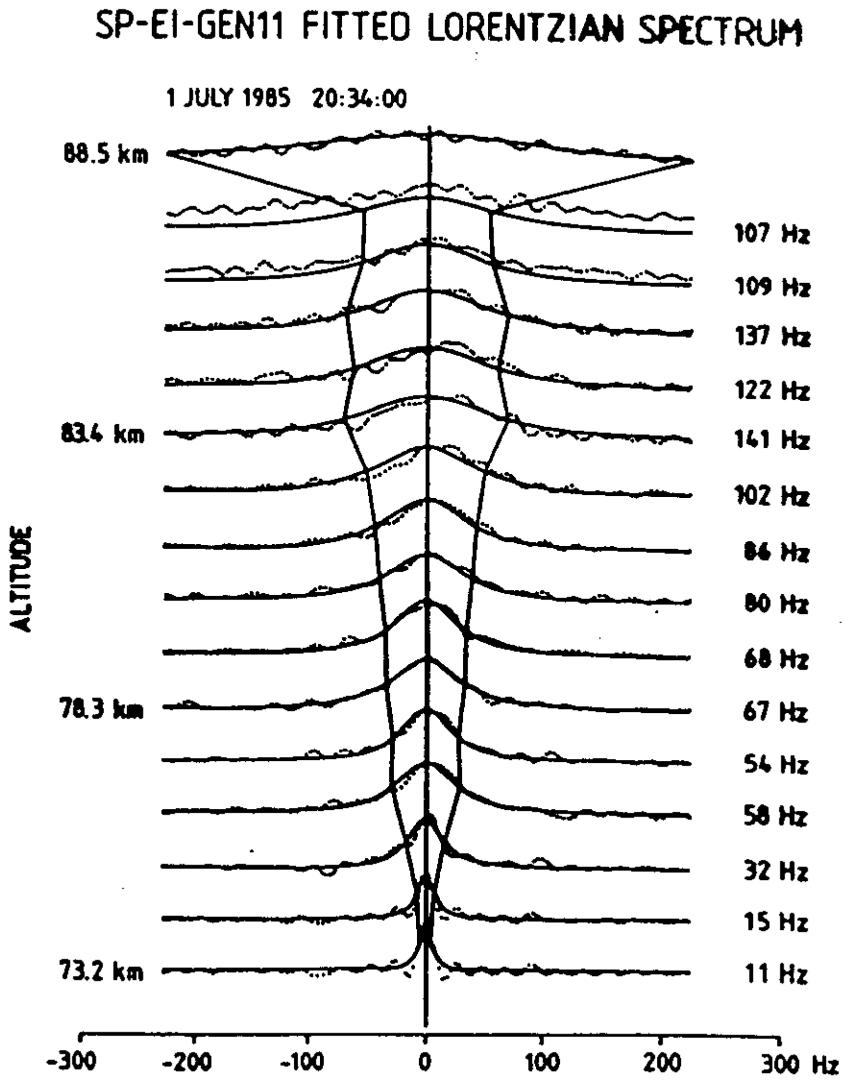

Fig. 18. *Spectra of D-region echoes, indicating a narrowing of the spectrum width between 85 and 87 km.*

E30

EISCAT VHF Radar (224 MHz)

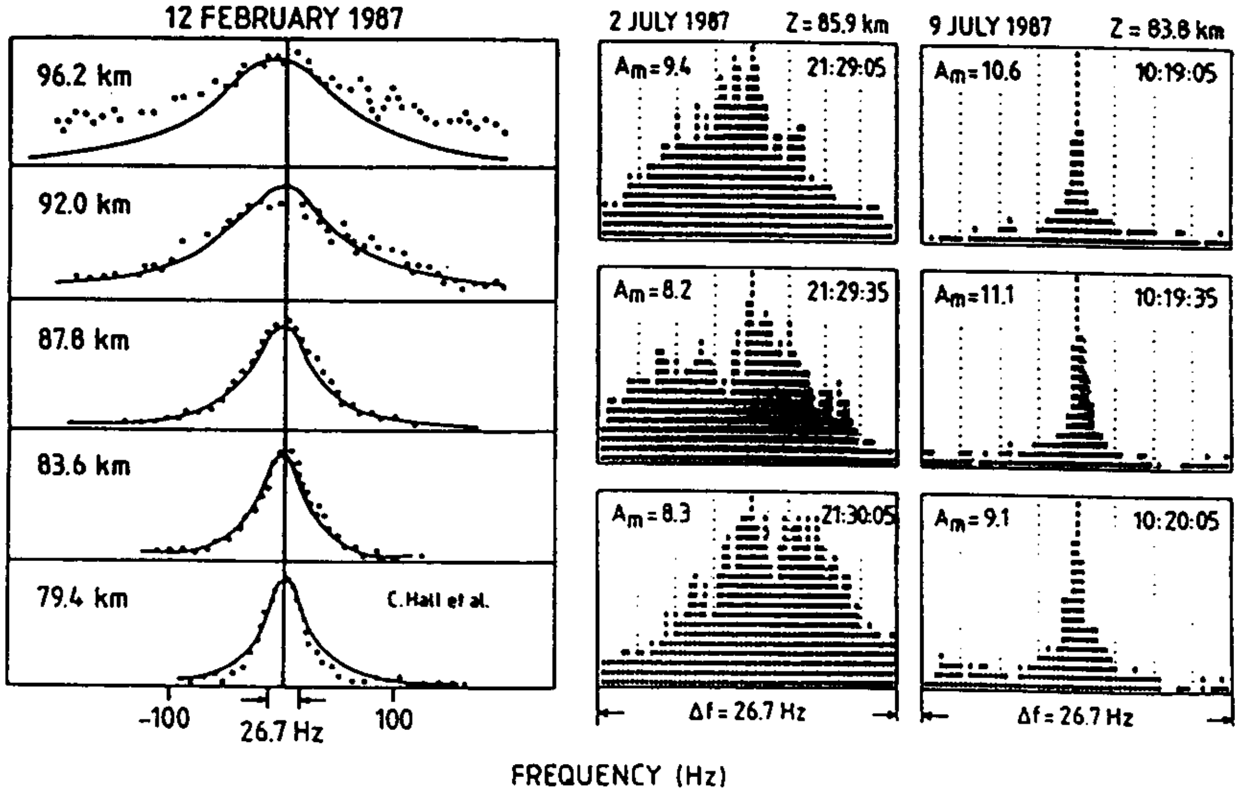

F 31

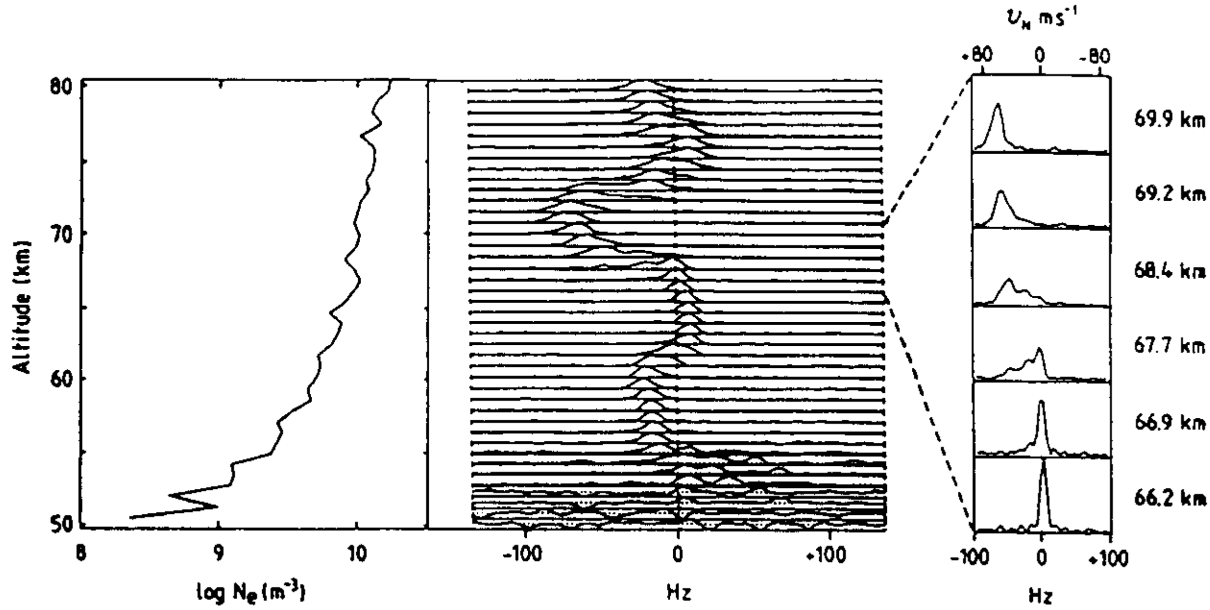

Fig. 1. EISCAT 224-MHz measurements from March 20, 1990, at 1330:50 UT (2-min

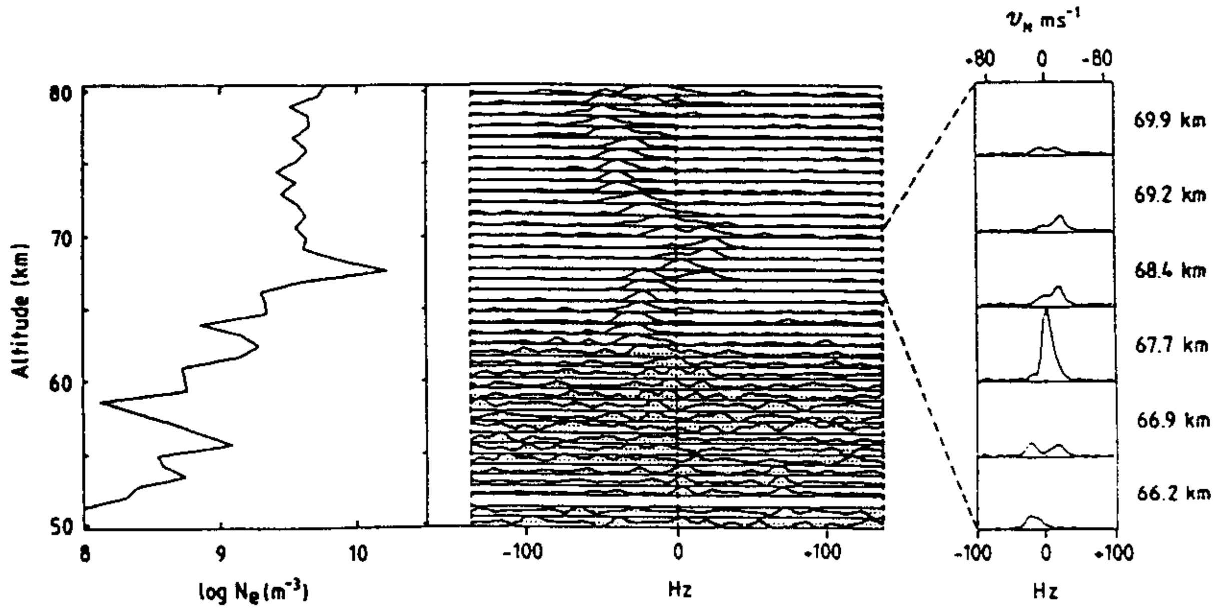

Fig. 2. As Figure 1, but for March 21, 1990, at 0610:10 UT. Note that the thin layer in the electron density profile near 68 km is due to increased backscatter from turbulence as discussed in the text and should not be interpreted as electron density.

MESOSPHERIC VHF RADAR ECHOES
(COLLISION DOMINATED)

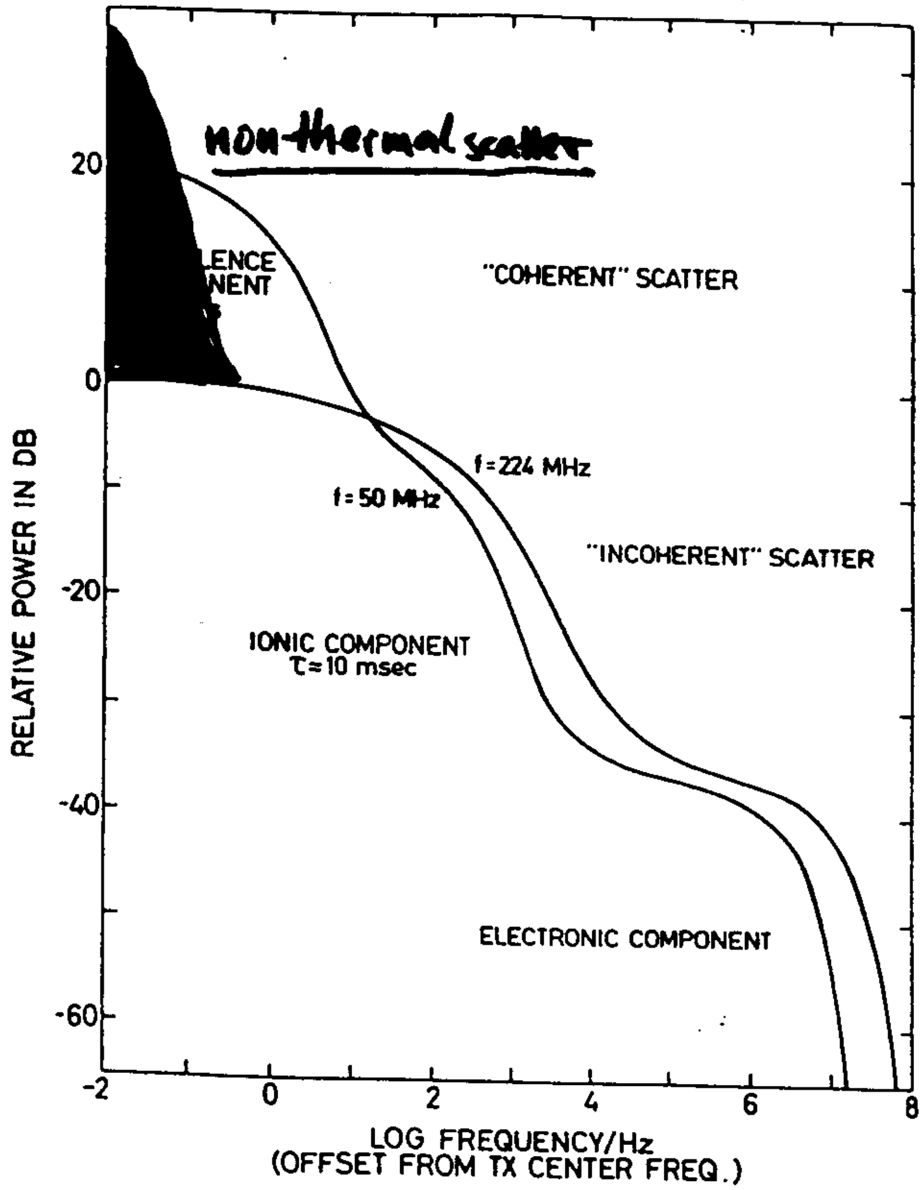

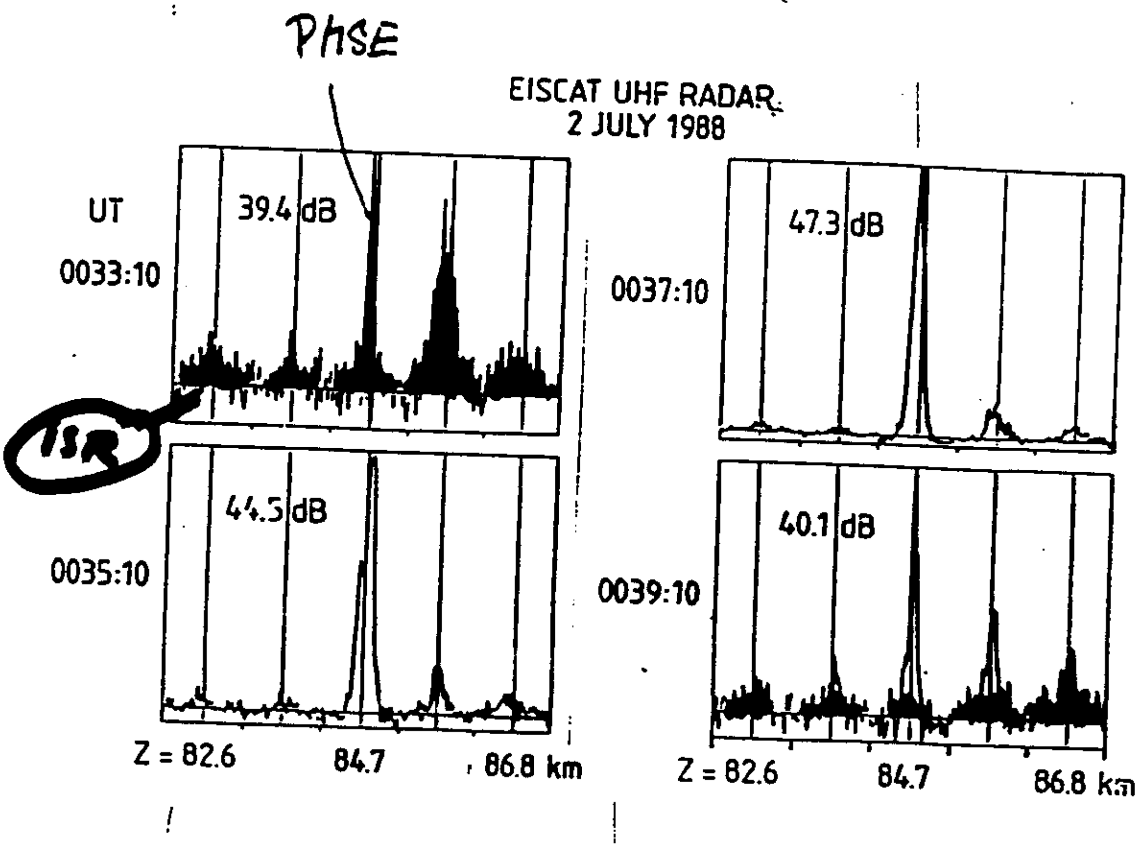
PMSE
EISCAT UHF RADAR
2 JULY 1988
UT
0033:10
39.4 dB
ISR
0035:10
44.5 dB
Z = 82.6
84.7
86.8 km
0037:10
47.3 dB
0039:10
40.1 dB
Z = 82.6
84.7
86.8 km

E34

When the ion-cyclotron frequency Ω_i is larger than the ion-neutral collision frequency ν_i the measured ion velocity v is affected by the plasma drift velocity caused by the electric field **E** and the magnetic field **B**. The measured ion drift velocity is

$$v = p \cdot \left(u + \frac{\Omega_i}{\nu_i} (u \times B) \right) + q \cdot \left(\frac{E}{B} + \frac{\Omega_i}{\nu_i} \frac{(E \times B)}{B^2} \right)$$

$$p = \nu_i^2 / (\Omega_i^2 + \nu_i^2)$$

$$q = \nu_i \Omega_i / (\Omega_i^2 + \nu_i^2)$$

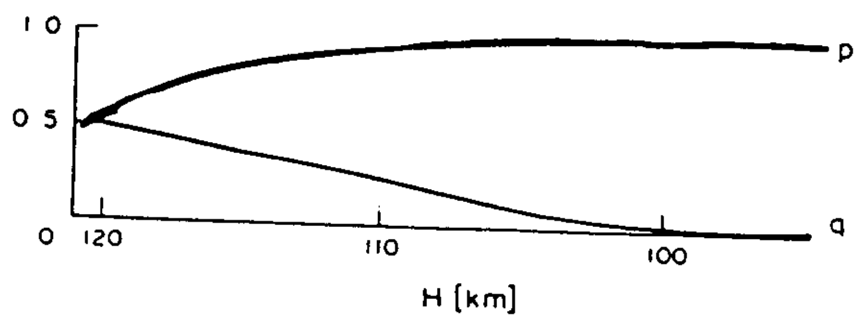

Below about 100 km, where p >> q, the measured ion drift v is usually equivalent to the neutral velocity u.

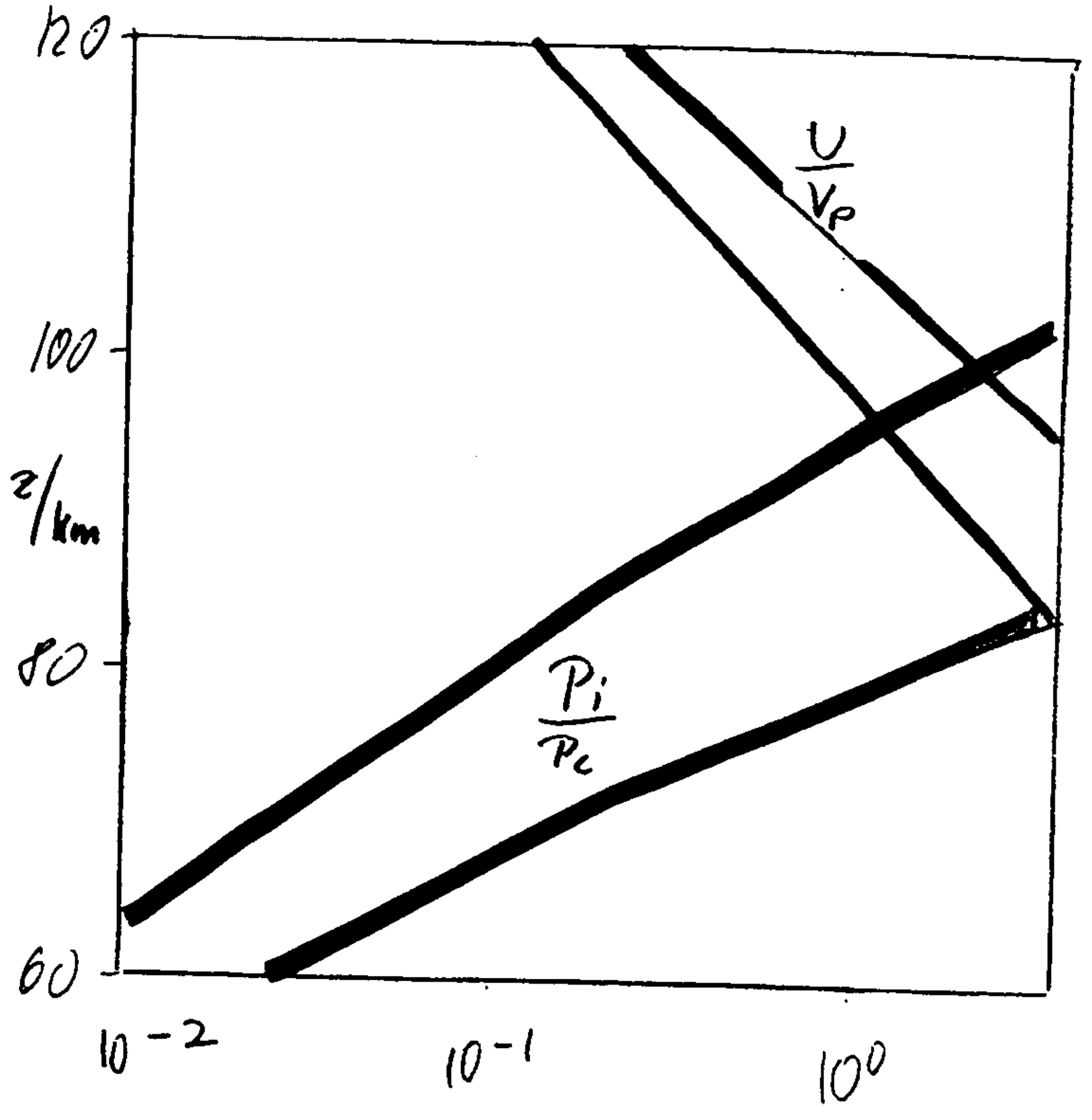

E26

From these basic parameters, N_e , u , T , λ^-, m_i , ν_i , and ρ_n , observed by incoherent scatter radar in the mesosphere, some derived parameters describing the middle atmosphere dynamics and aeronomy are deduced, as for instance:

Energy Input and Balance
(Joule, particle, radiation)
Winds, Tides and Gravity Waves
Momentum Transfer
Composition Changes
(production, loss, transport)

Typical resolutions are depending on the signal-to-noise ratio (i.e. the power-aperture product of the radar and the electron density):

Time resolution: 10 sec - 30 min
Height resolution: 150 m - 5000 m

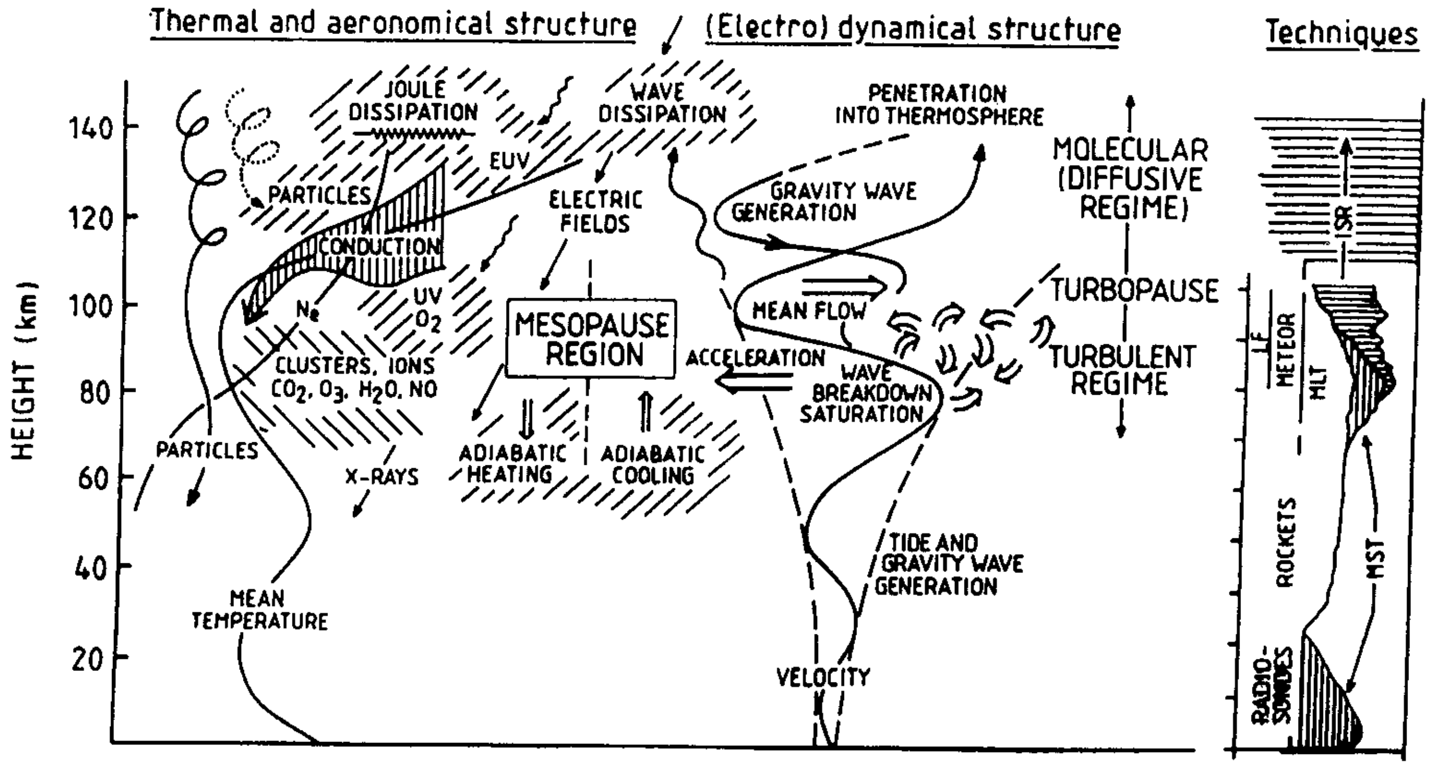
Thermal and aeronomical structure
(Electro) dynamical structure
Techniques
HEIGHT (km)
140
120
100
80
60
40
20
JOULE DISSIPATION
PARTICLES
CONDUCTION
EUV
UV
O_2
N_e
CLUSTERS, IONS
CO_2, O_3, H_2O, NO
PARTICLES
X-RAYS
MEAN TEMPERATURE
WAVE DISSIPATION
ELECTRIC FIELDS
MESOPAUSE REGION
ADIABATIC HEATING
ADIABATIC COOLING
PENETRATION INTO THERMOSPHERE
GRAVITY WAVE GENERATION
MEAN FLOW
ACCELERATION
WAVE BREAKDOWN SATURATION
TIDE AND GRAVITY WAVE GENERATION
VELOCITY
MOLECULAR (DIFFUSIVE REGIME)
TURBOPAUSE
TURBULENT REGIME
ISR
LF
METEOR
MLT
ROCKETS
MST
RADIO-SONDES

F3

D-region/mesosphere incoherent/coherent scatter

First significant observations

1974	Woodman and Guillen	MST, Jicamarca	50 MHz
1976	Mathews	ISR, Arecibo	430 MHz
1982	Balsley et al.	MST/PMSE, Poker Flat	50 MHz
1983	Luhman et al.	ISR, Chatanika	1296 MHz
1984	Kofman et al.	ISR, EISCAT	933 MHz
1987	Hall et al.	ISR, EISCAT	224 MHz
1988	Hoppe et al.	ISR/PMSE, EISCAT	224 MHz
1990	Röttger et al.	ISR/PMSE, EISCAT	933 MHz
1990	Collis et al.	ISR/MST, EISCAT	224 MHz
1992	Cho et al.	ISR/PMSE, So'strom	1296 MHz

D-region/mesosphere incoherent/coherent scatter:

1960	*Dougherty and Farley*	incoherent scattering
1963	*Moorcroft*	Debye length effects
1967	*Dougherty and Farley*	collisions
1969	*Evans*	review
1974	Woodman and Guillen	coherent scatter on 50 MHz at JRO
1976	Mathews	mesospheric tides at AO
1978	Harper	electron density, neutral wind
	Mathews	negative ions at AO
	Beynon and Williams	review
	Tepley and Mathews	collision frequency, temperature
1979	Ganguly et al.	negative ions
	Mathews and Bekeny	E_s, tides and vertical motions
	Banks	Joule heating
1980	Ganguly	dynamics, vert. energy flux
	Fukuyama and Kofman	negative ions increase scatter
1981	*Mathews and Tanenbaum*	negative ions
	Tepley et al.	intermediate layers
	Tepley et al.	temperatures, collision freq.
	Fukuyama	waves in the mesosphere
	Kockarts and Wisemberg	chemical fluctuations
	Forbes	tidal effects on chemistry
1982	Mathews et al.	diurnal variations
1983	*Wisemberg and Kockarts*	chemical fluctuations
	Luhman et al.	ISR and MST at Poker Flat
1984	Ganguly	heavy ion ledge
	Mathews	review
	Kofman et al.	first EISCAT D-region (UHF)
1985	Ganguly	sunrise-sunset (temperature, pos. ions)
	Tepley and Mathews	ion mass, temperature in E_s
	Ranta et al.	comparison with absorption
1986	Collis et al.	substorm effects on D-region

1987	Ganguly and Coco	theory - experiment equivalent
	Kelley et al.	Schmidt number effect (cluster ions)
	Hall et al.	first high lat. D-region (VHF)
	Hargreaves et al.	recombination rate
1988	Hoppe et al.	coherent scatter on 224 MHz (PMSE)
	Hall and Brekke	Schmidt numbers at mesopause
	Rastogi et al.	solar flare effect on 50 and 440 MHz
	Hall et al.	negative ions
	Collis et al.	heavy positive ions
1989	Hall, C.	high latitude review
	Chakrabarty and Ganguly	negative ions
	Huuskonen	collision freq. and temperature
1990	Collis and Röttger	high latitude review
	Collis and Rietveld	electron densities and negative ions
	Collis et al.	turbulence/incoherent scatter 224 MHz
	Röttger et al.	bite-out, coh. scat. 933 MHz (PMSE)
	Reid, G.C.	electron density bite-out
	Hall, C.	effect of heavy proton hydrates
	Havnes et al.	charged dust in the mesosphere
	Collis and Kirkwood	discrete ion layers
1991	Hansen et al.	spectral width deviations
	Burns et al.	chemical modelling
	Kirkwood et al.	E_s and sodium layers
1992	*Cho et al.*	charged aerosols
	Hagfors	dressed aerosols
	La Hoz	dusty plasma
	Turunen et al.	ion layers
	Cho et al.	coherent scatter on 1289 MHz
1993	Rietveld and Collis	negative ions, dynamics
	Cho and Kelley	coherent echoes (PMSE) review
	Mathews et al.	ion layers
	Rietveld et al.	dynamics during PCA
	Röttger	dynamics (SPE created?)
	Hines et al.	mesospheric motions (AIDA)
1994	*Klostermeyer*	two-ion ice particle model
	Röttger	EISCAT review
	Turunen, E.	high latitude review
	Cho et al.	charged aerosols
1995	Turunen, E.	high lat. D-region
	Mathews	ion layers
	Röttger	ISR-MST scatter review

EQUATORIAL IS/MST RADAR

[redacted]

The EISCAT Svalbard Radar
System Specifications 1995

	Location:	near Longyearbyen
	78°09'N, 16°03'E	on Spitsbergen, Svalbard
Operating Frequency:		500 MHz
Bandwidth:	Transmitting:	± 2 MHz
	Receiving:	± 10 MHz
Antenna:	Parabolic dish:	one (upgradable to >1)
	Beamwidth:	1.6° (one-way)
	Gain:	42 dBi
	Aperture:	≈ 500 m²
	Polarization:	circular
	Steerability:	all azimuths, 0-180 degrees elevation
Transmitter:	Peak Power:	0.5 MW, modular system (upgradable to 1MW)
	Average Power:	0.125 MW
	Tubes:	TV-klystrons (8)
	Pulse Length:	< 1 μs - 2 ms
	Modulation:	amplitude and phase coding
	Interpulse:	min. 0.1 ms
	Radar controller:	
	Program memory:	address space 20 bits 1 MW memory 32 bit control word with 100 ns resolution
Receiver:	Dual superheterodyne	
	Noise temp.:	≤ 20 K
	System Temp.:	≤ 100 K
	IF:	70 MHz ± 5 MHz
	Output channels:	up to 6
	ADC:	10 MHz min. 12 bit min.
	Complex digital mixer and filter:	
	Digital multiplier:	10 MHz bandwidth
	FIR filter:	10 MHz data rate 16 bit coeff. accur.
Digital Signal Processing:		Narrow- and wide-band
	Bus environment:	VME
	Host processor:	Sparc and 68040
	Lag profile proc.:	TMS 'C40x4 at 50 MHz
	Input data format:	16+16 bit complex
	Output data format:	32+32 bit complex
	Processing rate:	30 MOPS/channel
Total System Figure of Merit:		Peak Power x Aperture per System Temp.: 2.5 MW m²/K